Physics in Medicine & Biology

IPEM Institute of Physics and Engineering in Medicine

PAPER • OPEN ACCESS

Characterization of the PTB ultra-high pulse dose rate reference electron beam

To cite this article: Alexandra Bourgouin *et al* 2022 *Phys. Med. Biol.* **67** 085013

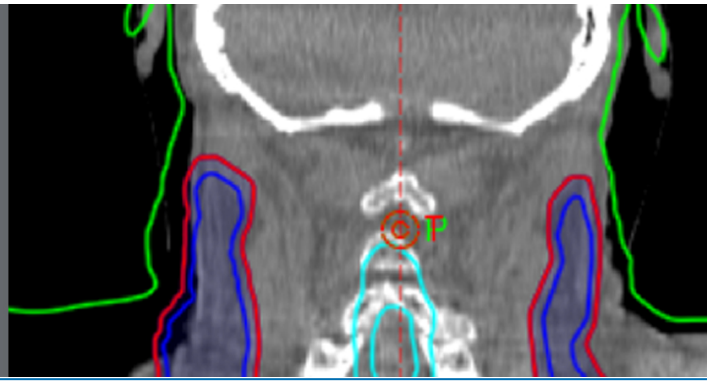

IOP Publishing Phys. Med. Biol. 67 (2022) 085013 https://doi.org/10.1088/1361-6560/ac5de8

Physics in Medicine & Biology

IPEM Institute of Physics and Engineering in Medicine

OPEN ACCESS

RECEIVED
19 November 2021

REVISED
17 February 2022

ACCEPTED FOR PUBLICATION
15 March 2022

PUBLISHED
8 April 2022

PAPER

Characterization of the PTB ultra-high pulse dose rate reference electron beam

Alexandra Bourgouin[1,*], Adrian Knyziak[2], Marco Marinelli[3], Rafael Kranzer[4,5], Andreas Schüller[1] and Ralf-Peter Kapsch[1]

[1] Physikalisch-Technische Bundesanstalt (PTB), Braunschweig, Germany
[2] Główny Urząd Miar (GUM), Poland
[3] University of Rome Tor Vergata, Industrial Engineering Dept., Rome, Italy
[4] PTW Dosimetry, Germany University Clinic for Medical Radiation Physics, Medical Campus Pius Hospital, Carl von Ossietzky University Oldenburg, D-26121 Germany
[5] University Clinic for Medical Radiation Physics, Medical Campus Pius Hospital, Carl von Ossietzky University Oldenburg, 26121 Germany
[*] Author to whom any correspondence should be addressed.

E-mail: alexandra.bourgouin@ptb.de, adrian.knyziak@gum.gov.pl, marco.marinelli@uniroma2.it, rafael.kranzer@ptwdosimetry.com, andreas.schueller@ptb.de and ralf-peter.kapsch@ptb.de

Keywords: Ultra-high dose rate, dosimetry for FLASH, Monte Carlo, diamond detector, electron beam

Abstract

Purpose. This investigation aims to present the characterisation and optimisation of an ultra-high pulse dose rate (UHPDR) electron beam at the PTB facility in Germany. A Monte Carlo beam model has been developed for dosimetry study for future investigation in FLASH radiotherapy and will be presented. *Material and methods*. The 20 MeV electron beams generated by the research linear accelerator has been characterised both in-beamline with profile monitors and magnet spectrometer, and in-water with a diamond detector prototype. The Monte Carlo model has been used to investigate six different setups to enable different dose per pulse (DPP) ranges and beam sizes in water. The properties of the electron radiation field in water have also been characterised in terms of beam size, quality specifier R_{50} and flatness. The beam stability has also been studied. *Results*. The difference between the Monte-Carlo simulated and measured R_{50} was smaller than 0.5 mm. The simulated beam sizes agreed with the measured ones within 2 mm. Two suitable setups have been identified for delivering reference UHPDR electron beams. The first one is characterised by a SSD of 70 cm, while in the second one an SSD of 90 cm is used in combination with a 2 mm aluminium scattering plates. The two set-ups are quick and simple to install and enable an expected overall DPP range from 0.13 Gy up to 6.7 Gy per pulse. *Conclusion*. The electron beams generated by the PTB research accelerator have shown to be stable throughout the four-months length of this investigation. The Monte Carlo models have shown to be in good agreement for beam size and depth dose and within 1% for the beam flatness. The diamond detector prototype has shown to be a promising tool to be used for relative measurements in UHPDR electron beams.

1. Introduction

The FLASH radiotherapy is a new treatment modality in which the prescribed dose is delivered with ultra-high pulse dose rate (UHPDR) beams in less than a second (Bourhis *et al* 2019b). The UHPDR is defined by a total dose delivered by a single pulse in the range between 0.6 Gy up to 10 Gy. The modality is in the early stage of development, but it has already shown advantage over conventional radiotherapy treatments as the adverse dose effect on healthy tissue is reduced. This is the so-called FLASH effect (Favaudon *et al* 2014, Montay-Gruel *et al* 2018, 2019, Bourhis *et al* 2019b, 2019a, Wilson *et al* 2020). The improved tissue response using FLASH modality can only be confirmed if the evaluation of the dose delivered by this modality is precise and accurate. Therefore, dosimetry is an essential aspect in the assessment of the FLASH effect.

To date, limited data are available on the functionality of standard dosimeters and how conventional code of practice (Andreo *et al* 2000, Almond *et al* 1999) should be modified to achieve the dosimetry precision required for research and clinical studies (Petersson *et al* 2017, Jaccard *et al* 2018, Favaudon *et al* 2019, Lansonneur *et al* 2019). Dedicated research in the field UHPDR dosimetry is therefore needed for the FLASH effect study to move forward. In that aim, the UHDpulse project, a project funded by the European Union within the EMPIR programme, has started in September 2019 (Schüller *et al* 2020). Within this project, the German national metrology institute (PTB) is mainly focused on the development of primary and secondary standards of absorbed dose to water in UHPDR electron beam, and to test the different detectors commercially available or under development for FLASH radiotherapy dosimetry purpose.

The pre-clinical research using UHPDR is usually performed in electron beams with modified (Schüler *et al* 2017, Lempart *et al* 2019, Ruan *et al* 2021) or dedicated (Jaccard *et al* 2018, Favaudon *et al* 2019, Moeckli *et al* 2021) linac (Kim *et al* 2021). Different techniques, mostly based on passive dosimeters, have been tested to characterise the UHPDR electron beams. Radiochromic films have been used in multiple studies for absolute and relative dosimetry, profile and depth dose curve measurements (Jaccard *et al* 2017, Petersson *et al* 2017, Schüler *et al* 2017, Lempart *et al* 2019, Konradsson *et al* 2020, Szpala *et al* 2021). They have the advantage to have a high spatial resolution, no dose-rate dependency and a complete 2D dose distribution can be obtained in a single pulse irradiation. However, they are passive dosimeter and the uncertainty on the dose measurement is high, 4% (Jaccard *et al* 2017, Konradsson *et al* 2020).

The PTB's Metrological Electron Accelerator Facility (MELAF) (Schüller *et al* 2019) is equipped with a research electron linear accelerator (linac) with the capacity to achieve the required ultra-high dose per pulse needed for FLASH research. The first main tasks of PTB within UHDpulse project were to establish a reference UHPDR electron beam at MELAF, to enable primary and secondary standard developments and to assess a dosimetry system for precise and accurate detector inter-comparison. In this aim, the research accelerator at PTB has been optimised to generate a 20 MeV electron reference beam in UHPDR mode.

The characterisation of the PTB reference UHPDR electron beam was carried out in parallel with the development of Monte Carlo model of the research accelerator. The in-vacuum electron beam, i.e. in the linac beamline, was characterised in the aim to generate a Monte Carlo model of the research linac. The model was used to further optimise the beam setup by modelling different source-surface distance (SSD), collimation and scattering plates.

For the characterisation of the beam in a water phantom, a diamond detector prototype was used. A prototype detector has been used rather than a commercially available diamond detector since saturation effect has been observed in UHPDR electron beam (Di Martino *et al* 2020). The prototype was specifically designed for UHPDR beam applications and had shown several advantages over the use of ion chambers or radiochromic films. Its response is linear in the desired range of dose per pulse (DPP), no correction factor for ion recombination effect is required and no conversion from depth ionization curve to a depth dose curve is needed. The diamond detector also has the advantage that the analysis of the data is simple and can be done in real-time. In addition, the diamond detector does not require additional equipment for signal reading contrarily to films.

This investigation aims to present the results of the optimisation and characterisation of the PTB's UHPDR electron beam and the results of a long-term beam stability study. This paper will also present the Monte Carlo model of the beamline built for the project along with its validation.

2. Material and methods

2.1. PTB research linear accelerator facility and equipments

The PTB MELAF is equipped with a custom-built research linear accelerator (linac) for fundamental dosimetry research. The linac can accelerate electrons to produce pulsed electron beams of nearly monoenergetic energies in a continuous range between 0.5 MeV up to 50 MeV with a spectrum width smaller than 0.05 MeV. The research linac facility consists of four rooms schematically shown in figure 1. One room is dedicated to the accelerating and energy separation components of the linac. Two rooms are dedicated for dosimetry experiments setups, one for low energy experiments (0.5–10) MeV and one for high energy experiments (10–50) MeV. The linac setting and output monitoring are done in a control room properly shielded for radiation safety.

For this project, the linac settings has been optimized to reach UHPDR with a 20 MeV electron beam. The beam pulse repetition frequency used was 5 Hz, and the pulse duration is 2.5 μs. More details of the research accelerator can be found in Schüller *et al* (2019). The in-vacuum beam, i.e. the electron beam travelling in the vacuum pipe of the beamline shown in figure 2, has been characterised in terms of beam energy and transverse shape. The energy fluence spectrum has been measured using a magnet spectrometer (figures 2(B) and (D)) (Renner *et al* 2014). The in-vacuum beam spatial shape was measured using two NEC beam profile monitors

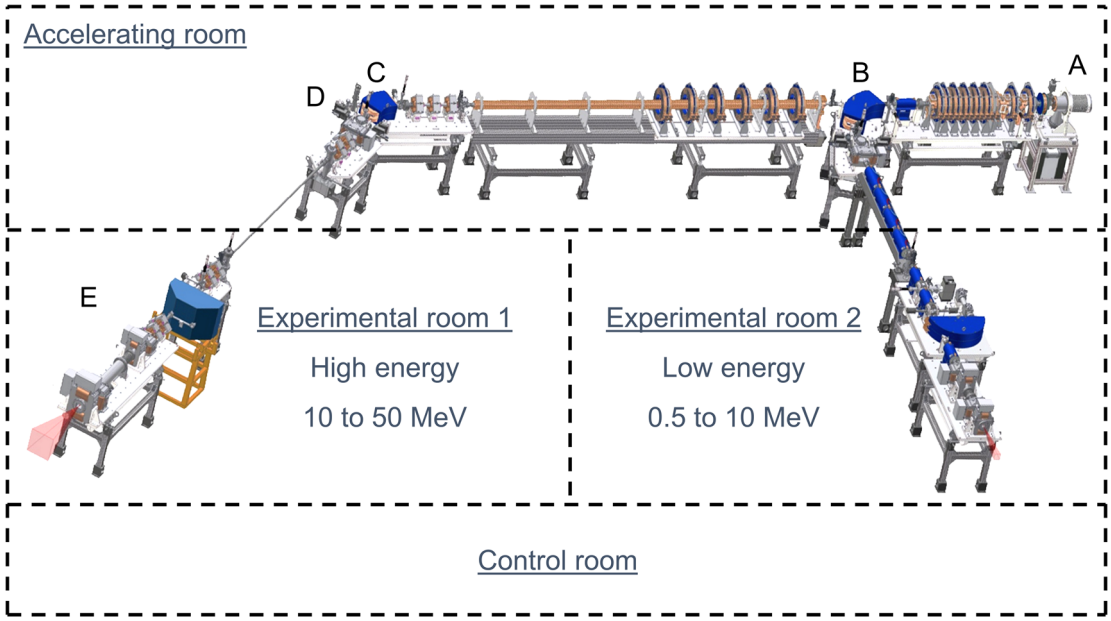

Figure 1. Schematic of the research linear accelerator of the MELAF facility at PTB. The dashed lines represent the room separation (not on scale). The following components are found in the accelerating room; (A) electron gun, (B) low energy bending magnet, (C) high energy bending magnet and (D) water-cooled movable jaws. The details of the high energy beamline labelled as (E) is shown in figure 2.

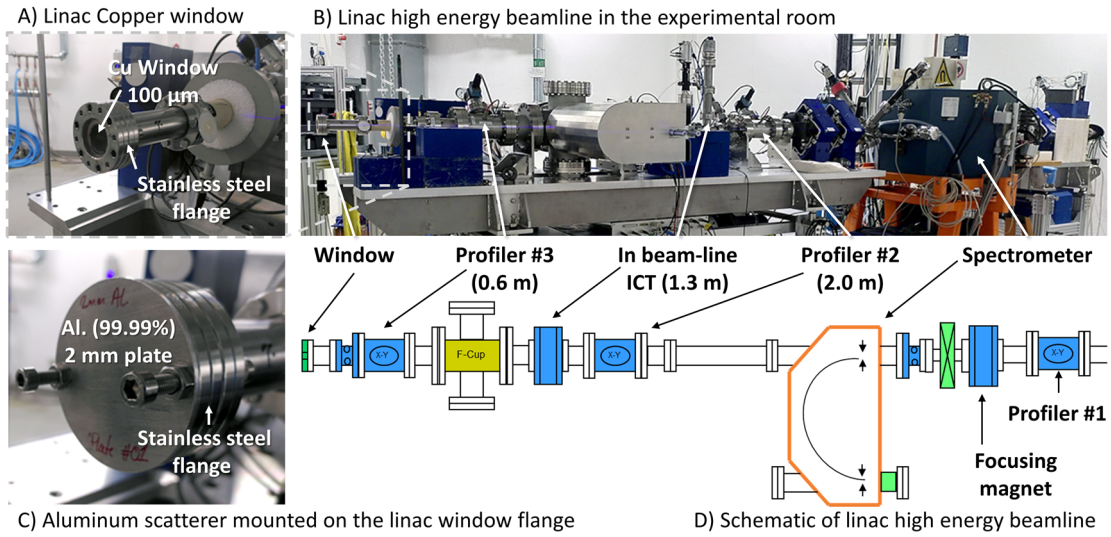

Figure 2. Pictures and schema of the PTB research linac high energy beamline, exit window and scattering plate. (A) Close-up picture of the linac 100 μm copper exit window. (B) Picture of the high energy beamline. (C) Picture of an aluminium scattering plate mounted on the exit window flange. (D) Schematic drawing of the high energy beamline. The distances indicated are up to the exit window.

(BPM80 monitors, National Electrostatics Corp., USA), labelled as profiler #2 and #3 in figures 2(B) and (D). The in-vacuum beam characterised has been used as input parameters for the Monte Carlo model.

The research linac is equipped with an in-flange integrating current transformer (ICT) (Bergoz, turns ratio 50:1) (Schüller *et al* 2017) as shown in figures 2(B) and (D) for beam monitoring. For separation of a monoenergetic beam and to bend the beam in the direction of the high energy beamline section (in experimental room 1, figure 1), the linac is equip with a high energy bending magnet. The electron beam exits the beamline vacuum pipe through a 100 μm thick copper window. For additional scattering, metal plates can be mounted on the exit window flange as shown in figure 2(C).

An important beam parameter for UHPDR electron beam dosimetry investigation is the DPP. To vary the DPP with the research linac, it is possible to change the accelerating settings (electron gun high voltage and RF

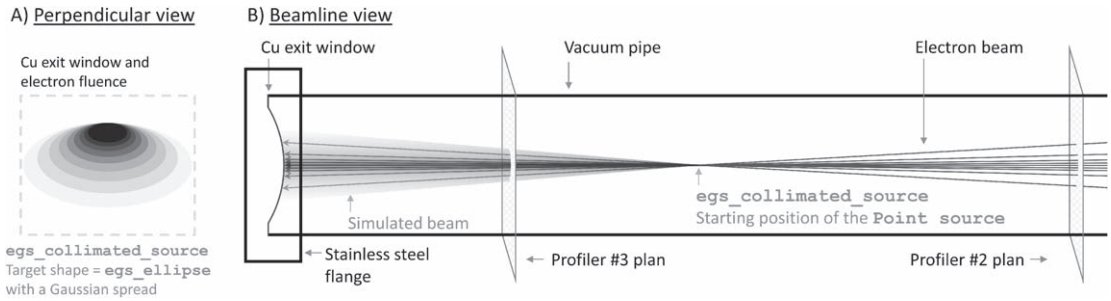

Figure 3. Schema of the linac vacuum beamline and the electron beam profile with an overlaid representation of the source simulated by EGSnrc Monte Carlo.

power), however, this could potentially change the beam characteristics (i.e. position of the beam axis, size and energy). The research linac is also equipped with a pair of water-cooled movable jaws positioned after the bending magnet (figure 1(D)). The jaws are moving and blocking the beam in the horizontal direction to create an adjustable slit width. The jaw position is measured using a potentiometer and the position coordinates are reinitiated every day by closing the slit. The jaws position, slit width, also vary the electron fluence which directly impacts the DPP, while minimally influencing the beam characteristics. To validate this assumption, the impact of the slit width on the beam characteristic was also investigated in the presented work.

2.2. Monte Carlo

Two Monte Carlo models of the beam have been developed using EGSnrc software toolkit, release v2020 (Kawrakow *et al* 2000), and FLUKA (Battistoni *et al* 2016). The Monte Carlo models were developed based on the energy fluence spectrum measured with the magnet spectrometer and the transverse profiles, horizontal and vertical, measured with the profilers #2 and #3. Both Monte Carlo models have been developed independently, the EGSnrc model was developed at PTB and the FLUKA model at the Central Office of Measures (GUM, Poland). PTB had provided the in-vacuum beamline characterisation of the research linac to GUM without further information about the EGSnrc model. The results obtained with the two Monte Carlo beam models have been compared to each other and to the relative measurement in water, which will be described below.

The EGSnrc was used to simulate lateral beam profiles in the beamline, in water and depth dose curves. Particles have been tracked down to a kinetic energy of 5 keV and no variance reduction was used. The EGSnrc beam source model was developed to match the measured in-vacuum beam FWHM at 0.6 m upstream to the linac exit window, i.e. to match the dimension at the position of the profiler #3. The beam source model selected was based on three observations from the measurement. First, the vertical beam profile is larger at profiler #2 than at profiler #3, which indicates that the in-vacuum beam is converging or focusing between the two profiles. Therefore, the EGSnrc beam source was modelled using egs_collimated_source which is a point source diverging to a target shape. The point source position was simulated to be between the two profilers according to the measured profile dimension, i.e. at 118 cm from the linac exit window. Secondly, as the horizontal beam profile is larger than the vertical one, the beam target shape was an ellipse defined at the position (0, 0, 0) to reproduce the different beam shapes measured depending on the slit width. Lastly, since the fluence is not uniform throughout the profile, a Gaussian angular spread was applied to the simulated diverging point source.

To validate the shape of the beam source model and to determine the proper ellipse dimensions for each slit width used in this investigation, a first set of EGSnrc simulations were done using the selected source shape and was compared to the in-vacuum beam profile measurements. The simulated geometry was a thin air layer, thickness of 2 mm, subdivided in 1 mm side voxels in transverse direction of the beam at 0.6 m from the geometry point (0, 0, 0). A thin layer of air was chosen to decrease the simulation time while minimally affecting the proportionality between energy deposited in the voxels (simulation) and the fluence (value measured with the profiler). The beam source model is schematically presented in the figure below.

For the simulation of the beam in water, the linac vacuum pipes are not included in the geometry and it starts at the exit window (defined at the position (0, 0, 0)) to simulate particle interactions in the 100 μm copper window. The trajectory of simulated electrons is therefore linear from the initial point source to the targeted ellipse shape, electron interaction with matter starting at the linac exit window. The beam source model used was the same as developed with the previously mentioned set of simulations. The water tank was simplified as a single water cube subdivided in layers of thickness 0.1 cm in depth direction. To obtain lateral dose profiles, the water

Table 1. List and description of the different electron beam setups investigated by EGSnrc Monte Carlo simulations.

Setup name	SSD (cm)	Collimation	Scattering plate
SSD50-00	50	None	None
SSD50-00c	50	PVC tube	None
SSD50-01c	50	PVC tube	Al. 1 mm plate
SSD70-00	70	None	None
SSD90-00	90	None	None
SSD90-02	90	None	Al. 2 mm plate

cube was also subdivided in cylinders with increment of 0.1 cm radius in the orthogonal direction to the beam axis.

The version 2011-3.0 of FLUKA (Battistoni *et al* 2016) was used for an independent beam model comparison. The advanced interface Flair 3.0-1 was used to calculate the absorbed dose in water phantom positioned at 70 cm from the linac exit window. The electron beam source was simulated as a 20 MeV beam using the BEAM card module with a Gaussian energy spread. A spatial Gaussian spread was also applied to the beam source which was simplified as a parallel beam in the FLUKA source model. The PRECISIO standard defaults set was used to configure the physical transport and interaction parameters of the simulations. The dose distribution was scored using the USRBIN scoring card in a water phantom of $30 \times 30 \times 30\,cm^3$ positioned at 70 cm from the source. The scoring volumes were voxels of $0.2 \times 0.2 \times 0.2\,cm^3$. To reach lower statistical uncertainty, the number of histories was set to 5×10^8 for each simulation with 5 cycles.

2.3. Beam setups

The EGSnrc model has been used to investigate a total of six different possible setups to enable different DPP ranges and beam sizes in water by using simple scattering plate, a cylindrical tube for collimation and different SSD position. To investigate the different possible setups, the application cavity was used to simulate depth dose curve and profile while giving information on the energy fluence spectrum at the water tank entrance window and at the depth of z_{ref} in water. The list of setups investigated is reported in table 1. The DPP range reach by changing the slit width, between 1 mm up to 20 mm, with an initial reference electron beam with an SSD of 70 cm was measured using alanine (Anton 2006) in the aim to estimate the absolute DPP range that could be achieved with different slit width for each setup investigated.

The collimation system investigated is a cylindrical PVC tube and is illustrated in figure 4. The tube's inner diameter is 5.0 cm. As the tube would need to be aligned over the linac exit flange, which has an outer diameter of 6.5 cm, the tube was selected to have an outer diameter of 7.5 cm. The tube was cut at the proper length to create a SSD of 50 cm between the linac exit window and the water tank entrance window once it was installed (water tank window touching the tip of the tube). PMMA and metal were discarded as material for the collimation tube since PMMA has shown to have poor radiation resistance when used in UHPDR and metal would have potentially created radiation safety issues. PVC was selected since it was available at a low cost in the desired dimension and easy to machine.

The scattering plates simulated were uniform plate of 1 mm or 2 mm thick made of 99.99% pure aluminium. This material was selected for its low atomic number, which is convenient for radiation protection (lower risk/level of activation). The scattering plate, when used, has been mounted to the beam line exit window stainless steel flange to ensure a perpendicular interception by the electron beam, shown in figure 2. The flange provided a reproducible distance of 7.6 mm between the copper exit window and the scattering plate.

2.4. Relative dose measurement in water

The relative dose measurement in water have been performed in a water tank installed on a translation table as illustrated in figure 4. The distance between the entrance window of the water tank and the beamline exit window, i.e. the SSD, was measured using a laser range finder ($\pm$ 3.0 mm, Bosch, Gerlingen Germany). The water tank used is made of 1 cm thick PMMA ($30 \times 30 \times 30\,cm^3$) walls. The entrance window is a 0.776 cm thick polycarbonate plate since PMMA has shown to accumulate radiation damage quickly in UHPDR electron beam. The scaling factor use to convert the entrance water tank window in equivalent water depth was the density of clear polycarbonate, $1.20\,g{\cdot}cm^{-3}$, as recommended by code of practice (Andreo *et al* 2000). The water tank is equipped with a motorized precise XYZ positioning system to position the dosimeter and can be adapted to accommodate different detectors.

The relative dosimetry measurement has been performed using a diamond detector prototype (B1). The prototype used in this investigation is a diamond Schottky diode detector designed for UHPDR beam

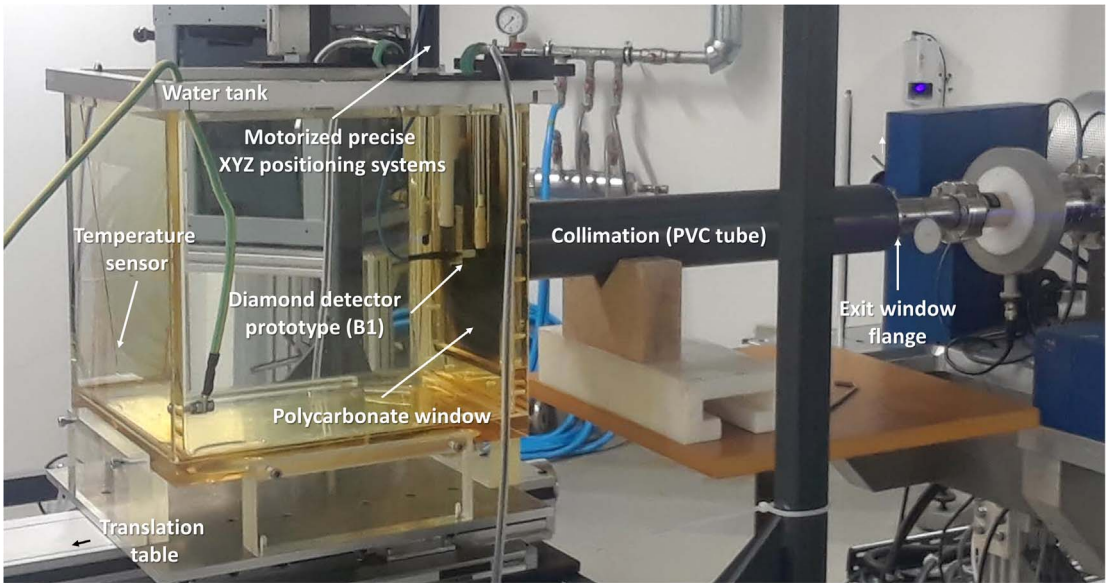

Figure 4. Picture of the experimental setup at a SSD of 50 cm using a PVC tube collimator with an aluminium scattering plate of 1 mm thick placed against the linac exit flange (at 0.76 cm from the exit window, not visible) and the water tank used at the PTB research accelerator during this investigation.

applications at the Rome Tor Vergata University in collaboration with PTW Freiburg (Kranzer *et al* 2022). The diamond prototype has a smaller series resistance and active volume to decrease DPP dose response dependency and to avoid saturation effect. The sensitive volume of the detector is a synthetic single crystal diamond whose active volume is 1.0 μm thick and a 0.7 mm diameter. It is waterproof and the measuring point is at a water equivalent depth of 1 mm below its top surface.

The DPP response of the diamond detector prototype has been characterised against the in-flange ICT monitoring system which has been calibrated by means of alanine (Bourgouin *et al* 2020). This characterisation will be presented in a second paper. The conclusion of this investigation was that the linear response range of this diamond detector prototype is up to about 2.5 Gy per pulse. For the non-linear dose response range, a correction factor based on the diamond detector signal and the expected response from alanine absolute dose measurement was evaluated. The maximum deviation was estimated to be less than 5% in the range of DPP in the presented investigation.

The advantages of using such a diamond detector prototype for the relative measurements reported in the present study are: a small sensitive volume in directions orthogonal and parallel to the beam axis, the capability for real-time measurements and a linear response up to 2.5 Gy per pulse. Another advantage is that the water to diamond stopping power ratio can be assumed as constant in good approximation for the energy range investigated here. Therefore, percentage depth dose curves can be directly obtained from the relative depth measurement if the absolute DPP throughout the depth remains in the linear dose response range of the detector. Other influencing effects on the depth dose measurement, such as the effective point of measurement or delta rays, can be neglected as the sensitive volume of the diamond is small.

The beam characterisation of the six beam setups evaluated by `EGSnrc` Monte Carlo simulation were compared to relative dose measurement in water. For each setup, a depth dose curve, and two beam profiles, horizontal and vertical, at z_{ref} were measured using the diamond detector prototype. These measurements were performed using slit width of 4 mm to ensure a linear dose response of the detector throughout the profile and depth measurement curve for most investigated setups while keeping linac setting constant. For beams where the signal exceeded the linear dose response range of the diamond (SSD50-00 and SSD50-00c), the measurements were corrected as mentioned earlier. The DPP depends on the beam setups and varies between 0.3 Gy per pulse (SSD90-02) up to 5.0 Gy per pulse (SSD50-00c).

The profiles and depth dose curve were acquired while the linac was running continuously. The profiles were taken in a radius of 6.0 cm radius from the beam centre by steps of 1.0 cm and 0.5 cm in the 1.0 cm radius (23 lateral position measured). For the depth dose curve, measurements were carried out from 0.1 cm of the water tank entrance window up to 10 cm depth (11.03 cm depth of equivalent water depth). A total of 20 depths were measured. For each profile position and depth, 10 points of measurements were taken for an acquisition time of 10.0 s (5 pulses averaging) which led to an average statistical uncertainty of better than 0.05% at z_{ref} at the beam centre. The scanning time for a profile was 5 min and 4 min for a depth dose curve.

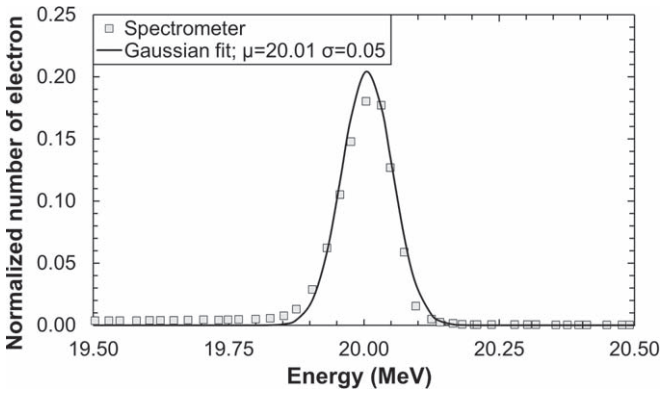

Figure 5. The normalised energy fluence spectrum of the high-energy electron beam optimized for the PTB research in UHPDR pulse mode. The normalized energy fluence spectrum measured is represented by the squares and the line is the Gaussian best fit.

After validating the results obtained by simulation, two beams setup were selected as UHPDR electron beam reference for the long-term beam stability study. For this study, a measurement procedure with the diamond detector prototype was developed to evaluate and monitor the: beam centre position, depth of R_{50} and beam size. The impact of the slit width on the beam centre position and beam size was also monitor during the stability study. The measurement procedure was as following: the diamond detector prototype B1 was installed and positioned in the water tank and moved in the horizontal and vertical direction (orthogonal to the beam) to a fixed position marked by the laser system installed in the experimental room. For the positioning of the detector depth in water, the outer surface of the detector was moved against the inner surface of the water tank polycarbonate window. A depth dose curve and an initial horizontal and vertical profile at z_{ref} were measured with the slit width of 4 mm. The diamond was re-centred according to the centres of the measured lateral beam profiles and a second profile was taken for validation. The beam profile in both directions were taken for slit width of 12 mm and 20 mm to evaluate the change in beam size and beam centre position due to slit width.

2.5. In-water beam characterisation formalism

The electron beams were characterised in terms of beam size, beam quality specifier (R_{50}) and flatness. The beam size is defined as the full width at half maximum (FWHM), i.e. the distance between the points at which the dose amounts to 50% of the maximum dose in horizontal and vertical directions, orthogonal to the beam direction. The beam quality specifier in UHPDR electron beam is the same as defined in conventional code of practice, R_{50}, which is the depth on the beam axis where the absorbed dose is equal to 50% of the maximum dose. The flatness of the beam, i.e. the maximum deviation in the lateral beam profile compared to the central dose, was evaluated within a field size of 1.5 cm radius. The reference depth for absorbed dose measurements, z_{ref}, is also defined as in conventional code of practice (Almond *et al* 1999, Andreo *et al* 2000):

$$z_{\mathrm{ref}} = 0.6 \cdot R_{50} - 0.1 \text{ cm}.$$

3. Results and discussion

3.1. In-vacuum beam characterisation

The normalised energy fluence spectrum reported in figure 5 has been measured by the magnet spectrometer. The measurement has been performed for the highest possible fluence (beam current of 230 nC), i.e. with fully opened slit. The measured energy fluence spectrum was approximated by a Gaussian shape for the `EGSnrc` simulation. According to these results, it was decided to model the source energy distribution as a Gaussian function, with a mean energy of 20.006 MeV and a standard deviation of 0.047 MeV. As the energy fluence spectrum was assumed to be constant up to the slit position (linac accelerating settings constant) and since Monte Carlo calculation had shown no significant difference in the results between a monoenergetic beam of 20 MeV and the selected source energy distribution model, it was decided to use the same energy fluence spectrum for all slit width simulated.

The in-vacuum electron beam profiles have been measured using NEC beam profile monitors (profiler) closest to the exit window; number #2 (2.0 m upstream from the exit window) and #3 (0.6 m upstream from the exit window) as illustrated in figure 2. The beam profiles measurements have been done for slit width between 0 and 20 mm by steps of 4 mm and for a fully opened slit (about 48 mm). The measurements and

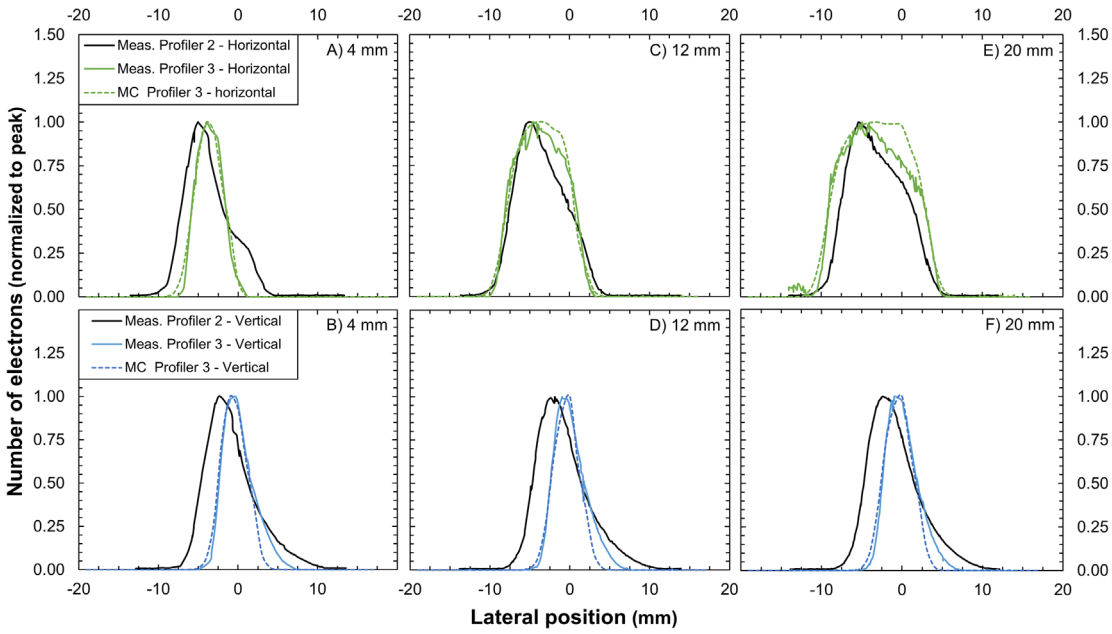

Figure 6. Measured and simulated in-vacuum electron beam profiles. Horizontal profiles (upper plots) and vertical profiles (lower plots) are reported for different slit width; (A) and (B) 4 mm, (C) and (D) 12 mm and (E) and (F) 20 mm. The black solid lines are the measurements at the profiler #2, the coloured solid lines are the measurements at the profiler #3, and the dashed lines is the in-vacuum beam profiles generated by EGSnrc simulation at the position of profiler #3.

Table 2. Measured dimension of the electron beam in the vacuum beamline of the PTB research accelerator.

Slit width (mm)	Vertical axis		Horizontal axis	
	Beam size (mm)		Beam size (mm)	
	Profiler #2	Profiler #3	Profiler #2	Profiler #3
	FWHM	FWHM	FWHM	FWHM
4	6.0	4.1	5.5	4.3
12	6.2	4.4	7.6	9.0
20	6.2	4.2	9.7	13

EGSnrc beam source profiles in-vacuum are shown in figure 6. For clarity purposes, only the results for slit width of 4 mm, 12 mm and 20 mm are shown. The measured beam size and positions are listed in table 2.

As illustrated in figure 6, the vertical beam profiles measured for different slit width are very similar, while the horizontal profiles are found to be changing significantly with the slit width. As the linac slit's jaws are moving and blocking the beam in the horizontal direction, it was therefore expected to observe a change in the beam horizontal profile and a stable shape in the vertical direction.

3.2. UHPDR electron beam characterization in water

In the aim to validate the EGSnrc beam source model presented in the above section and the beam setup as listed in table 1, measurements of depth dose curves and beam profiles have been carried out in water. The results of the simulation and measurement of the beam setups for linac slit width of 4 mm are shown in figure 7. In table 3, the results of the simulation are presented. The values in backet are the difference between the simulation and the measurement. The difference between the reference depth, z_{ref}, of the beam setup SSD70-00 (see reference in table 1) was less than 1 mm between the EGSnrc and FLUKA simulation and within 0.5 mm of the measured value. The profile flatness was measured to be 9.3% within 1.5 cm radius of the lateral beam centre at z_{ref} and was found to be 9.4% and 8.9% from EGSnrc and FLUKA simulations respectively. The FWHM of lateral profiles was measured to be 8.04 cm and were found to be 8.23 cm and 8.04 cm from EGSnrc and FLUKA respectively.

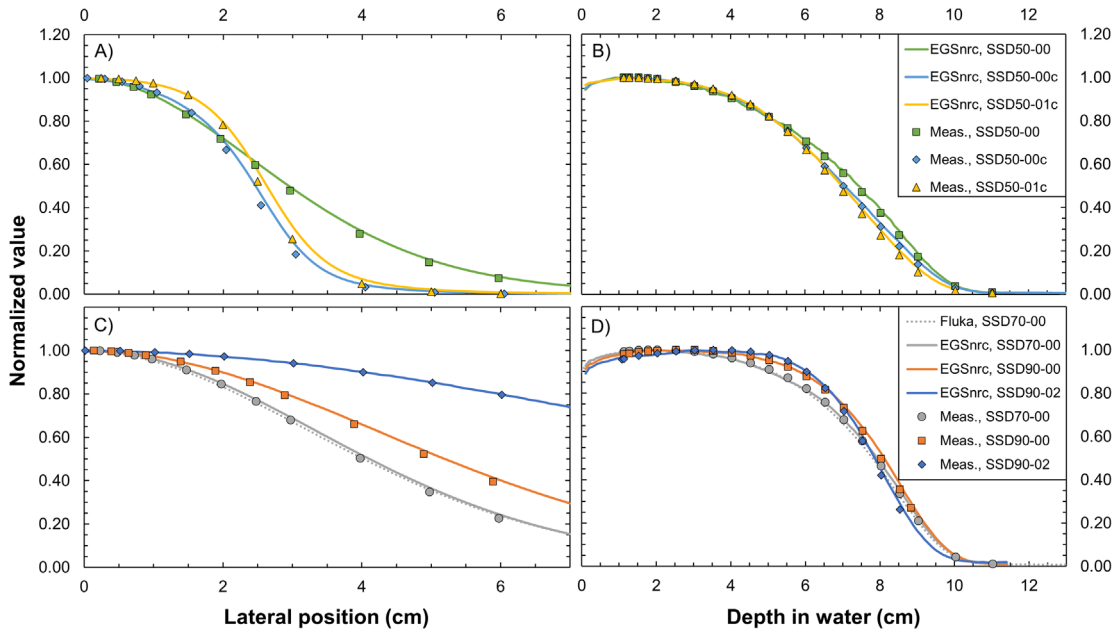

Figure 7. Simulated and measured lateral beam profiles and depth dose curves of the setups listed in table 1 separated into four separate plots for clarity. (A) and (C) are the lateral beam profile at depth of z_{ref}. Due to symmetry, only half of the profiles are shown. (B) and (D) show the percentage depth dose curves.

Table 3. Expected beam characteristic of the simulated setups for the reference electron UHPDR beam at PTB facility. These beams have been simulated using `EGSnrc` cavity application with the beam model source for linac slit width of 4 mm. The expected dose range have been calculated based on initial absolute dosimetry of the beam setup SSD70-00 using Alanine. The number in bracket is the difference between the measured and simulated value. The energy spectra have been simulated using `EGSnrc` cavity application. The detailed description of the investigated setups is reported in table 1.

	Setup	SSD50-00	SSD50-00c	SSD50-01c	SSD70-00	SSD90-00	SSD90-02
	Dose range (Gy per pulse)	[1.7, 12]	[2.0, 15]	[1.0, 7.3]	[0.90, 6.7]	[0.56, 4.2]	[0.13, 1.0]
	R_{50} (mm)	74.5(−0.9)	70.6(−0.4)	69.8(−0.9)	79.2(−0.5)	81.2(−1.0)	78.6(−0.8)
	z_{ref} (mm)	43.7(−0.5)	41.4(−0.2)	40.9(−0.5)	46.5(−0.3)	47.7(−0.6)	46.2(−0.5)
	R_{95} (mm)	32.2(0.3)	33.6(0.4)	34.2(0.7)	42.0(1.1)	49.9(0.7)	55.4(−0.4)
	Flatness at depth z_{ref}	17(0.4)%	14(0.6)%	8.0(−0.2) %	9.4(−0.04) %	5.9(0.00)%	1.5(−0.05)%
	FWHM at z_{ref} (mm)	60(−1)	49(−2)	53(−2)	82(−2)	103(−2)	208(1)
Energy at tank surface (MeV)	Spectral peak	19.9	19.8	19.5	19.8	19.8	19.0
	Average	19.7	18.6	17.1	19.6	19.5	18.4
Energy at z_{ref} (MeV)	Spectral peak	11.8	12.2	11.6	11.2	10.9	10.2
	Average	9.2	9.2	8.3	8.5	8.2	7.6

From the `EGSnrc` simulation and measurement results shown in figure 7, the beam setup SSD70-00 and SSD90-02 were identified as the most suitable beam for stability study of the UHPDR electron beam. The combined use of two setups enables a wider range of DPP, from about 0.13 Gy up to 6.7 Gy and relatively flat beam. These setups are also very simple and quick to install and mostly within the linear dose response range of the B1 detector. In addition, it was found that the collimated beam was not practical as its installation required multiple iterations of profile measurements and positioning verifications to ensure that the tube is well aligned with the electron beam.

Another practical advantage of using these two beam setups is the very similar reference depth for both selected beams, 46.5 mm (SSD70-00) and 46.2 mm (SSD90-02), a difference of 0.3 mm. Although the average energy at the water tank window of the beam is smaller for the setup SSD90-02 as listed in table 3, the beam size also impacts the depth of R_{50} and thus z_{ref}. The difference between the reference depth for both setups have been measured to be 0.4(2) mm, consistent with the value obtained by simulation. From the simulation, it was decided to establish the reference depth at 46.5 cm in water for both beam setups.

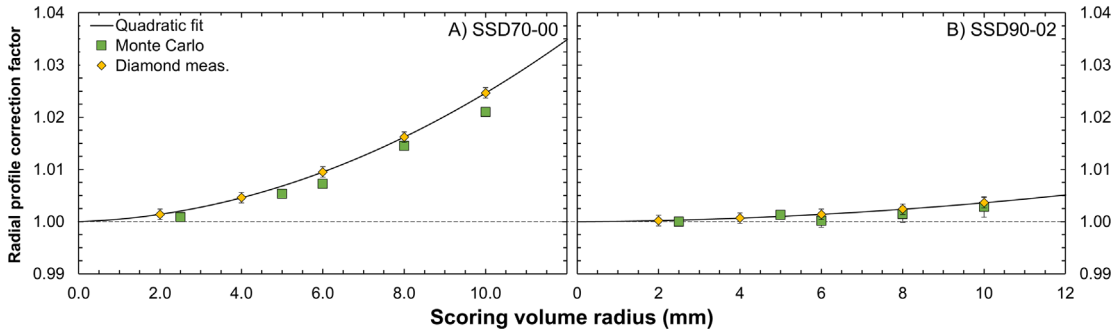

Figure 8. Correction factor for volume averaging effect from the lateral variation of the beam intensity.

Table 4. Characterization of the impact of the linac slit width on the horizontal beam size and relative dose deposited at the reference measurement point, normalized to dose measured with a slit width of 4 mm for the beam setup SSD70-00.

		FWHM horizontal (mm)		Normalized signal	
Slit width	z_{ref} (±0.1 mm)	MC	Meas. (±0.4)	MC (±0.6%)	Meas. (±0.3%)
1 mm	46.6	81.9	79.6	1.009	1.008
4 mm	46.6	82.4	79.9	1	1
8 mm	46.6	82.5	80.6	0.994	0.985
12 mm	46.7	82.6	80.4	0.988	0.981
16 mm	46.6	83.7	80.9	0.968	0.976
20 mm	46.7	84.5	81.0	0.956	0.972

Due to the flattening free setup of both selected reference electron beams, a volume averaging effect in the radial direction is expected during measurement for detectors with different radius in the orthogonal direction of the beam. To estimate the influence of the radial non-uniformities of the beam profile, Monte Carlo simulations have been performed in water. The scoring volumes simulated were 1.0 mm thick water disks centred at the depth of z_{ref} with radius between 1.0 mm up to 10.0 mm. The simulated dose deposited was normalized to the smallest disk radius size to estimate the beam radial volume averaging correction factor. To compare the simulated correction factor results with measurement, a Gaussian fit was performed on the measured profile. From this Gaussian fit, it was possible to calculate the expected correction factor for the same range of sensitive (scoring) volume. The results of the values simulated and estimated from beam lateral profile measurements are shown in figure 8 along with a quadratic fit. The correction factor was estimated to be smaller than 1.0010(10) for sensitive volumes with radius smaller than 1.6 mm and 5.0 mm in the orthogonal direction of the beam for the setup SSD70-00 and SSD90-02 respectively. This correction should be therefore taken into consideration for future dosimetric investigation using the beam setup SSD70-00.

As shown in in figure 6, the in-vacuum horizontal beam profile can change significantly with the slit width. To investigate the impact of the horizontal beam size at the beam exit window on the dose in water, the beam profile in water at z_{ref} was simulated using `EGSnrc` and compared to measurement using the diamond detector prototype B1 for the setup SSD70-00, the results are shown in table 4. For the beam setup SSD70-00, the change in slit width results in a variation of the measured FWHM of the profile in water of 1.4 mm, while the in-vacuum horizontal beam size at profiler #3 increase by about 9 mm between slit width of 4 mm and 20 mm. The smaller change in water was expected due to electron scattering in water.

The variation of the beam size, due to the variation of the slit width, doesn't have a significant impact on the depth of z_{ref}. However, although the beam size changed by less than 1.5 mm, measurement show a change of 3.6(4)% in the normalized signal at reference measurement point. Therefore, a non-linear relationship is to be expected between the ICT monitoring signal, proportional to the in-vacuum beam fluence, and the dose deposited in water from varying the slit width. This effect is considered to be due to the change in the divergence of the beam in the beamline. This effect was also measured for the beam setup SSD90-02 and the change in the normalized signal to the in-beamline currant was 0.81(5)%.

The `EGSnrc` simulation study of the impact of the slit width predicted a 2.6 mm change in the beam size, 1.2 mm larger than the value obtained by the measurement. Also, a 5.3(8)% signal variation at the centre of the beam is expected from Monte Carlo calculation a difference of 1.7(9)% with the value calculated from

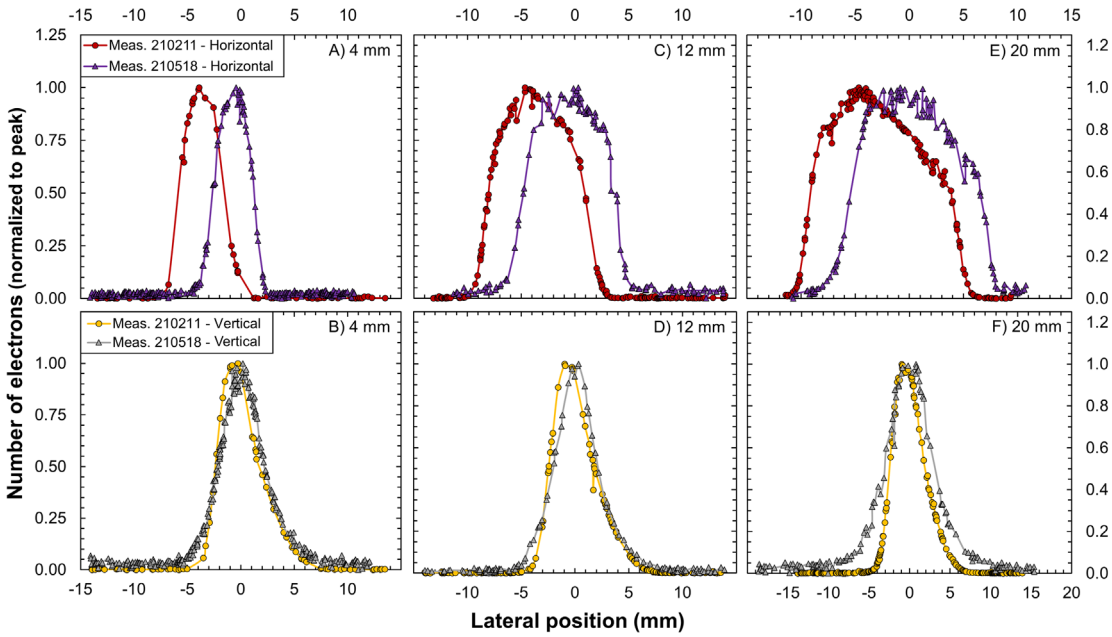

Figure 9. Comparison between the in-vacuum beam profile measured with the profiler #3 in February and May 2021. The panels, (A) and (B) are the profiles measured when using a 4 mm slit width setting, (C) and (D); 12 mm, and (E) and (F); 20 mm.

measurement. It should be noted that the EGSnrc only includes the impact of the beam size at the window and does not include the beam centre translation which was also observed and will be discussed below. These results highlight the limitation in the EGSnrc beam source model.

The ratio of the diamond prototype B1 signal measurement, normalized to the ICT signal for slit width of 4 mm, for both beam setups was measured to be 0.139(2). This ratio between the two beam setups is partly explained by the difference in the SSD used, a decrease of 40% in dose deposited, and the presence of the 2 mm aluminium scattering plate which significantly increases the divergence of the beam. From EGSnrc simulation, a ratio of 0.145 was expected. The 5% difference could be explained by the difference in the beam size in water at z_{ref} simulated compared to the one measured as shown in table 4. This difference is not observed for setup SSD90-02 as the beam size is considerably wider, FWHM of about 208 mm, compared to the setup SSD70-00, FWHM of about 80 mm.

3.3. Beam stability and monitoring

The stability of the beam setup and linac output was investigated for 6 weeks on the two selected beam setups SSD70-00 and SSD90-02. The measurements were performed between April and June 2021 on 17 days. These measurements were compared to measurement carried out four months earlier, in February and March 2021, which the EGSnrc model was based and presented in earlier sections.

3.3.1. In beamline

The in-vacuum electron beam profile characteristics are presented in figures 9 and 10. In figure 9, a comparison is reported between the beam profiles measured with slit width of 4 mm, 12 mm and 20 mm in February and May 2021. In figure 10, the measured in-vacuum electron beam FWHM and centre position are reported. The results presented for the month of May 2021 in figure 10 are the average value measured throughout that month and the error bar represent the maximum and minimum value measured during the linac stability investigation.

As shown in figures 9 and 10, the most significant change observed in the in-vacuum beam characteristics between the measurement carried out in February and May 2021 is the central position of the horizontal profile. This was expected as the steerer magnet settings for central positioning of the in-vacuum beam were reoptimized to centre the beam in April 2021. As shown in figure 10, the change of this setting had a minor impact, smaller than 0.6 mm, on the other in-vacuum beam characteristics.

3.3.2. In water stability measurement

The following paragraphs will present the result of the beam stability study in water carried out by using the diamond detector prototype (B1). For the setup SSD70-00, the z_{ref} was evaluated, on average over the 17 days of measurement perform between April and June 2021, to be at a depth of 45.8 mm and the standard deviation was

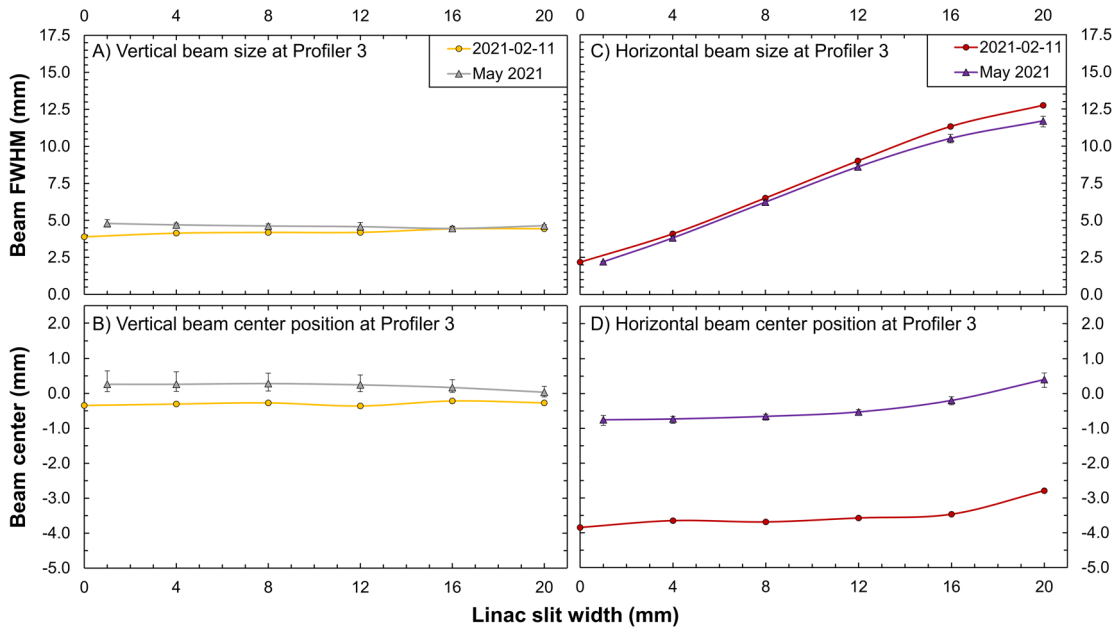

Figure 10. In-vacuum beam profile characteristics measured in February and in May 2021, in horizontal and vertical direction as a function of the slit width. The beam size (FWHM) is reported in the upper plots (A) and (C), while the beam centre position is reported in the lower ones (B) and (D). The presented data for February represent a single day of measurement while the data presented for May 2021 is the average over all the measurement carried out during the month. The error bars are the lower and higher measurement observed during the stability study of May 2021.

Table 5. Beam size (FWHM) and centre position in water as measured by the diamond B1 during the investigation in May 2021.

		SSD70-00		SSD90-02	
	Slit width	Horizontal	Vertical	Horizontal	Vertical
Beam centre position, relative to room laser (mm)	4	−2.0(4)	0.6(5)	−2.8(3)	−0.5(4)
Beam centre position, relative to slit width 4 mm (mm)	4	0.1(1)	0.0(1)	0.2(2)	0.0(4)
	12	0.0(3)	0.0(2)	0.2(3)	0.1(3)
	20	−1.0(4)	0.1(1)	−0.9(5)	0.1(1)
FWHM (mm)	4	80.0(3)	80.3(3)	208.6(3)	208.3(3)
	12	80.3(3)	80.1(4)	209.3(5)	208.8(4)
	20	81.0(3)	80.4(3)	210.2(4)	209.4(5)
Flatness over 3 cm Ø (%)	4	90.4(1)	90.4(1)	98.49(4)	98.49(4)
	12	90.9(1)	90.8(1)	98.50(4)	98.50(5)
	20	91.3(1)	91.2(1)	98.51(4)	98.50(4)

measured to be 0.1 mm. This measurement is consistent with the measurement performed in February 2021. The measured z_{ref} for the setup at SS90-02 was 45.4 mm with a standard deviation of 0.05 mm, also consistent with previous measurement. The consistency between measurement of z_{ref} between February to June 2021 indicated a stability in beam energy and size. The largest deviation of the z_{ref} measured during the 17 days of measurement was 0.3 mm, therefore, depth positioning uncertainty can be considered nonsignificant for UHPDR electron beam measurement at PTB. For consistency in the measurement, the z_{ref} was kept at 46.5 mm for both setups, i.e. the value obtained by EGSnrc Monte Carlo simulation.

The result of the beam monitoring, lateral beam size and centre position, is presented in table 5 for both setups, SSD70-00 and SSD90-02, for different slit width (4 mm, 12 mm and 20 mm). The first line is the beam centre evaluated when the diamond was positioned following the room laser system. The centre position presented in the second line of table 5 is relative to the beam centre when the slit width is 4 mm. These values are evaluated once the coordinates of the water tank motorized precise XYZ positioning system have been reinitiated following the beam centre measured, which are presented in the first line of table 5. The number in brackets indicated the standard deviation measured during the 6 weeks of beam stability study.

As shown in first line of table 5, the beam centre evaluated when the diamond is centred with the laser system is consistent between the two setups. The beam centres while the slit width are at 12 and 20 mm, relative to position 4 mm, is as it was expected from the in-vacuum beam measurement shown in figure 10. The beam

centre for slit width 12 mm is unchanged, but a 1 mm difference is observed for the slit width 20 mm. The measurement of the beam sizes presented in table 5 is consistent with the measurement done in March 2021 within the observed standard deviation (number in brackets). In the case of the measured vertical beam, due to the scattering in water, although the beam size remains stable at the linac beamline, the vertical profile in water slightly changes as well. The change in beam size is consistent for both studied setups.

3.4. Results summary

The EGSnrc Monte Carlo beam source has been modelized as 20 MeV electron beam with a Gaussian energy distribution with a sigma of 0.047 MeV following the measurement using magnet spectrometer. Based on the transverse beam shape characterisation in the linac beamline, the beam source was modelled as a diverging point source at 118 cm from the 100 μm copper exit window with a target ellipse shape. The EGSnrc Monte Carlo simulation of the beam size, flatness and depth dose curve in water of six different beam setups have shown to be consistent with relative measurement using a diamond detector prototype within 2 mm for the beam size (FWHM), 0.6% for the flatness and 1.0 mm for the depth dose curve (calculated R_{50}).

From simulations and measurement in water, two beam setups were selected as reference beam; one at a SSD of 70 cm and one at a SSD of 90 cm in combination with a 2 mm thick aluminium scattering plate. These two beam setups enable an expected range of DPP between 0.13 Gy up to 6.7 Gy and the beam profile FWHM are respectively about 8.0 cm and 20.8 cm. As both beam setups are not using any flattening filter, the lateral averaging effect were calculated and was found to be smaller than 1.0036(10) for sensitive volume radius smaller than 1.0 cm in the beam setup SSD90-02. As the beam setup SSD70-00 as a smaller beam profile size, the correction can reach a value of 1.0247(10) for sensitive volume radius of 1.0 cm.

The stability of the linac in-vacuum beam and the two selected beam setups as reference beams have been monitored for 6 weeks. The in-vacuum beam size and central position has shown to be stable within 0.4 mm. The beam profile and depth dose curve were measured to be stable at the sub-millimetric level.

For each beam setups, the DPP is varied by changing the width of the slit created by a pair of water-cooled jaws positionned right after the bending magnet of the research linac. By changing the slit width, it is possible to change the in-vacuum beam currant. However, the in-vacuum beam characterisation has shown that it also impacts the beam size by 8.7 mm. The effect of changing the slit width has shown to have an impact of less than 1.5 mm on the beam size for both reference beam setups. However, as the divergence of the beam changes in the beamline, the relationship between in-beamline currant (monitoring ICT signal) and the dose deposited at the reference point is no longer linear. From Monte Carlo simulation and measurement, the deviation from linearity was evaluated to be up to 3.9(1)% for the reference beam SSD70-00 and up to 0.81(5)% for the reference beam SSD90-02.

4. Conclusion

In this investigation, the PTB research linac in-vacuum electron beam characterisation based on two NEC beam profile monitors and magnet spectrometer has been presented. These measurements have been used as an input for the development of EGSnrc and FLUKA Monte Carlo models of the beam source from the research accelerator at PTB. The models have been used to simulate in water measurement and were compared to the results obtained by using a diamond detector prototype designed for UHDR applications. The comparison has shown that the precision of the Monte Carlo models is in good agreement for beam size and depth dose and within 1% for the beam flatness.

The EGSnrc model has been used to simulate a total of six different electron beam setups using different SSDs, scattering plates and collimation system. The six setups have been characterised in water using the diamond detector prototype. From this investigation, two setups have been identified as suitable for delivering reference UHPDR electron beams for future PTB research in the scope of the UHDpulse project. The two selected reference beams were obtained at a SSD of 70 cm and at a SSD of 90 cm in combination with a 2 mm thick aluminium scattering plate positioned at the exit window of the beam line, respectively. The two beams are quick and simple to install and enable an overall DPP range from 0.13 Gy up to 6.7 Gy. From the Monte Carlo investigation, it was estimated that a DPP up to 15 Gy could be achieved using an SSD of 50 cm and a PVC collimator, however, the beam flatness would be not better than 14% within 1.5 cm radius in the centre of the beam.

During the investigation, the stability of the beam/research accelerator setting was studied. The electron beams generated by the research linac have shown to be stable during the four-months length of this investigation. The diamond detector prototype used in the present investigation has shown to be a promising tool for relative dosimetry in UHPDR electron beams. The real time detector response is characterised by a good spatial resolution, due to the small sensitive volume of the detector.

Acknowledgments

The authors thank Olaf Tappe for machining the water tank and the scattering/collimation system and we are also grateful for his useful advice during designing of the difference beam setup. We thank Christoph Makowski for the operation of the electron accelerator. The assistance of Markus Meier in the preparation of the experiments is gratefully acknowledged.

Conflict of interest

Rafael Kranzer is employee of PTW Freiburg. Marco Marinelli signed a contract with PTW-Freiburg involving financial interests deriving from the PTW microDiamond 60 019 dosimeter commercialization. The remaining authors declare that the research was conducted in the absence of any commercial or financial relationships that could be construed as a potential conflict of interest.

Funding

This project 18HLT04 UHDpulse has received funding from the EMPIR programme co-financed by the Participating States and from the European Union's Horizon 2020 research and innovation programme.

ORCID iDs

Alexandra Bourgouin https://orcid.org/0000-0001-6429-4122
Rafael Kranzer https://orcid.org/0000-0003-4063-0413
Andreas Schüller https://orcid.org/0000-0002-0355-299X

References

Almond P R, Biggs P J, Coursey B M, Hanson W F, Huq M S, Nath R and Rogers D W O 1999 AAPM's TG-51 protocol for clinical reference dosimetry of high-energy photon and electron beams *Med. Phys.* **26** 1847–70

Andreo P, Burns D T, Hohlfeld K, Huq M S, Kanai T, Laitano F, Smith V G and Vynckier S 2000 Absorbed dose determination in external beam radiotherapy: an international code of practice for dosimetry based on standards of absorbed dose to water *IAEA Technical Report Series* No 398 International Atomic Energy Agency, Vienna

Anton M 2006 Uncertainties in alanine/ESR dosimetry at the physikalisch-technische bundesanstalt *Phys. Med. Biol.* **51** 5419–40

Battistoni G *et al* 2016 The FLUKA code: an accurate simulation tool for particle therapy *Front. Oncol.* **6** 116–39

Bourgouin A, Schüller A, Hackel T, Kranzer R, Poppinga D, Kapsch R-P and McEwen M 2020 Calorimeter for real-time dosimetry of pulsed ultra-high dose rate electron beams *Front. Phys.* **8** 400–9

Bourhis J *et al* 2019a Clinical translation of FLASH radiotherapy: why and how? *Radiother. Oncol.* **139** 11–7

Bourhis J *et al* 2019b Treatment of a first patient with FLASH-radiotherapy *Radiother. Oncol.* **139** 18–22

Di Martino F *et al* 2020 FLASH radiotherapy with electrons: issues related to the production, monitoring, and dosimetric characterization of the beam *Front. Phys.* **8** 481–94

Favaudon V *et al* 2014 Ultrahigh dose-rate FLASH irradiation increases the differential response between normal and tumor tissue in mice *Sci. Transl. Med.* **6** 245ra93–245ra93

Favaudon V, Lentz J M, Heinrich S, Patriarca A, de Marzi L, Fouillade C and Dutreix M 2019 Time-resolved dosimetry of pulsed electron beams in very high dose-rate, FLASH irradiation for radiotherapy preclinical studies *Nucl. Instrum. Methods Phys. Res. A* **944** 162537

Jaccard M, Durán M T, Petersson K, Germond J-F, Liger P, Vozenin M-C, Bourhis J, Bochud F and Bailat C 2018 High dose-per-pulse electron beam dosimetry: commissioning of the Oriatron eRT6 prototype linear accelerator for preclinical use *Med. Phys.* **45** 863–74

Jaccard M, Petersson K, Buchillier T, Germond J-F, Durán M T, Vozenin M-C, Bourhis J, Bochud F O and Bailat C 2017 High dose-per-pulse electron beam dosimetry: usability and dose-rate independence of EBT3 Gafchromic films *Med. Phys.* **44** 725–35

Kawrakow I, Rogers D W O, Mainegra-Hing E, Tessier F, Townson R W and Walters B R B 2000 EGSnrc toolkit for Monte Carlo simulation of ionizing radiation transport (https://nrc-cnrc.github.io/EGSnrc/) (https://doi.org/10.4224/40001303)

Kim M M, Darafsheh A, Schuemann J, Dokic I, Lundh O, Zhao T, Ramos-Mendez J, Dong L and Petersson K 2021 Development of Ultra-High dose rate (FLASH) particle therapy *IEEE Trans. Radiat. Plasma Med. Sci.* **7311** 1–12

Konradsson E, Ceberg C, Lempart M, Blad B, Bäck S, Knöös T and Petersson K 2020 Correction for Ion recombination in a Built-in monitor chamber of a clinical linear accelerator at Ultra-High dose rates *Radiat. Res.* **194** 580–6

Kranzer R, Schüller A, Bourgouin A, Hackel T, Poppinga D, Lapp M, Looe H K and Poppe B 2022 Response of diamond detectors in ultra-high dose-per-pulse electron beams for dosimetry at FLASH radiotherapy *Phys. Med Biol.* **67** 075002

Lansonneur P, Favaudon V, Heinrich S, Fouillade C, Verrelle P and De Marzi L 2019 Simulation and experimental validation of a prototype electron beam linear accelerator for preclinical studies *Phys. Med.* **60** 50–7

Lempart M, Blad B, Adrian G, Bäck S, Knöös T, Ceberg C and Petersson K 2019 Modifying a clinical linear accelerator for delivery of ultra-high dose rate irradiation *Radiother. Oncol.* **139** 40–5

Moeckli R, Gonçalves Jorge P, Grilj V, Oesterle R, Cherbuin N, Bourhis J, Vozenin M C, Germond J F, Bochud F and Bailat C 2021 Commissioning of an ultra-high dose rate pulsed electron beam medical LINAC for FLASH RT preclinical animal experiments and future clinical human protocols *Med. Phys.* **48** 3134–42

Montay-Gruel P *et al* 2019 Long-term neurocognitive benefits of FLASH radiotherapy driven by reduced reactive oxygen species *Proc. Natl. Acad. Sci. USA* **166** 10943–51

Montay-Gruel P *et al* 2018 X-rays can trigger the FLASH effect: ultra-high dose-rate synchrotron light source prevents normal brain injury after whole brain irradiation in mice *Radiother. Oncol.* **129** 582–8

Petersson K, Jaccard M, Germond J-F, Buchillier T, Bochud F, Bourhis J, Vozenin M-C and Bailat C 2017 High dose-per-pulse electron beam dosimetry - a model to correct for the ion recombination in the advanced markus ionization chamber *Med. Phys.* **44** 1157–67

Renner F, Schwab A, Kapsch R P, Makowski C and Jannek D 2014 An approach to an accurate determination of the energy spectrum of high-energy electron beams using magnetic spectrometry *J. Instrum.* **9** P03004

Ruan J L *et al* 2021 Irradiation at Ultra-high (FLASH) dose rates reduces acute normal tissue toxicity in the mouse gastrointestinal system *Int. J. Radiat. Oncol. Biol. Phys.* **111** 1250–61

Schüler E, Trovati S, King G, Lartey F, Rafat M, Villegas M, Praxel A J, Loo B W and Maxim P G 2017 Experimental platform for ultra-high dose rate FLASH irradiation of small animals using a clinical linear accelerator *Int. J. Radiat. Oncol. Biol. Phys.* **97** 195–203

Schüller A *et al* 2020 The european joint research project UHDpulse—metrology for advanced radiotherapy using particle beams with ultra-high pulse dose rates *Phys. Med.* **80** 134–50

Schüller A, Pojtinger S, Meier M, Makowski C and Kapsch R P 2019 The metrological electron accelerator facility (MELAF) for research in dosimetry for radiotherapy *IFMBE Proc.* vol 68 (Springer) 589–93

Szpala S, Huang V, Zhao Y, Kyle A, Minchinton A, Karan T and Kohli K 2021 Dosimetry with a clinical linac adapted to FLASH electron beams *J. Appl. Clin. Med. Phys.* **22** 50–9

Wilson J D, Hammond E M, Higgins G S and Petersson K 2020 Ultra-high dose rate (FLASH) radiotherapy: silver bullet or fool's gold? *Front. Oncol.* **9** 1563–74